Biosensors and Bioelectronics 141 (2019) 111417

Contents lists available at ScienceDirect

Biosensors and Bioelectronics

journal homepage: www.elsevier.com/locate/bios

ZnO-based nanostructured electrodes for electrochemical sensors and biosensors in biomedical applications

Nagaraj P. Shetti[a,**], Shikandar D. Bukkitgar[a], Kakarla Raghava Reddy[b,*], Ch. Venkata Reddy[c], Tejraj M. Aminabhavi[d]

[a] Electrochemistry and Materials Group, Department of Chemistry, K. L. E. Institute of Technology, Affiliated to Visvesvaraya Technological University, Gokul, Hubballi, 580030, Karnataka, India
[b] School of Chemical and Biomolecular Engineering, The University of Sydney, Sydney, NSW, 2006, Australia
[c] School of Mechanical Engineering, Yeungnam University, Gyeongsan, 712-749, South Korea
[d] Department of Pharmaceuticals, Soniya College of Pharmacy, Dharwad, 580 002, Karnataka, India

ARTICLE INFO

Keywords:
Biosensors
Zinc oxide
Nanostructures
Electro-activity
Infectious diseases
Biomedical applications

ABSTRACT

Fascinating properties of ZnO nanostructures have created much interest due to their importance in health care and environmental monitoring. Current worldwide production and their wide range of applications signify ZnO to be a representative of multi-functional oxide material. Recent nanotechnological developments have stimulated the production of various forms of ZnO nanostructures such as nano-layers, nanoparticles, nanowires, etc. Due to their enhanced sensing properties, improved binding ability with biomolecules as well as biological activities have enabled them as suitable candidates for the fabrication of biosensor devices in the biomedical arena. In this review, the synthesis of ZnO nanostructures, mechanism of their interaction with biomolecules and their applications as sensors in health care area are discussed considering the biosensors for molecules with small molecular weight, infectious diseases, and pharmaceutical compounds.

1. Introduction

Recent developments in nanotechnology and their applications in biomedical area has led to developments of new techniques in areas of clinical diagnostics (Medawar-Aguilar et al., 2019; Kumar et al., 2013), environmental monitoring (Xu et al., 2017), health monitoring (Satish et al., 2017), food safety (Li et al., 2009), pharmaceutical analysis (Shetti et al., 2018, 2019 a,b,c; Devarushi et al., 2018; Bukkitgar et al., 2016a, 2016b, 2016c, 2017, 2018a, 2018b, 2019) and fundamental biological research (Ouhenia-Ouadahi et al., 2016). Bulk materials lack some unique physiochemical properties such as reactivity, adsorption, and a high surface-to-volume ratio, which has led to the development of cultured nanostructured materials (NSMs) for analytical applications where they can provide not only high sensitivity but also provide a valuable platform for the analysis of single-molecular activity (Patil et al., 2018; Haque et al., 2018; Reddy et al., 2009a, 2009b, 2010). The synthesis of NSMs with unique properties and functionality has provided a convenient platform to develop novel analytical probes, which upon exposure to the targeted molecules, trigger the production of analytical signals that can be measured (Wang et al., 2015a).

Semiconducting metal oxides have been extensively used as efficient NSMs in high-performance electronics, energy conversion/storage, and environmental remediation applications (Hu et al., 2013). Among the various metal oxide materials, ZnO has attracted considerable attention due to its commendable properties such as low cost, high abundance, and wide band gap. ZnO belongs to the direct and wide band gap metal oxide semiconductor material. It consists of hexagonal wurtzite crystal structure offering an easy growth of various 1-D micro and NSMs. Unique piezoelectric properties due to noncentrosymmetric crystal structure with Zn^{+2} and O^{-2} polar surfaces make ZnO more interesting for developing smart technologies such as piezo photocatalysis, piezotronics, and piezoelectronics (Yin et al., 2015).

Simple illumination with UV light produces oxygen vacancies onto the surface of ZnO, which can alter the intrinsic properties such as super-hydrophobicity to ultra-hydrophilicity and vice versa, increasing n-type conductivity, and other physio-chemical properties, thereby enabling their utilization in various interdisciplinary research (Djurisic and Leung, 2006). In addition, ZnO has been widely applied in devices such as supercapacitors, sensors, photocatalysis, and solar cells (Son et al., 2014; Wang et al., 2015b; He et al., 2011). The nontoxicity and

* Corresponding author.
** Corresponding author.
E-mail addresses: npshetti@kleit.ac.in (N.P. Shetti), reddy.chem@gmail.com (K.R. Reddy).

https://doi.org/10.1016/j.bios.2019.111417
Received 10 March 2019; Received in revised form 1 June 2019; Accepted 4 June 2019
Available online 08 June 2019
0956-5663/

compatibility of ZnO with human skin have allowed the use of ZnO as additives in textile industries and surfaces that are contacting human flesh. Further, the use of ZnO in the area of biomedical is not a new one and one can find its utilization since the ancient period. Zinc-fly ash was prominently used in the ancient period to cure fatal illness (Craddock, 2000). It is one of the most important mineral nutrients for the human body, controlling > 300 metabolic functions (Haase et al., 2008).

Furthermore, properties such as self-cleansing, antimicrobial activity and compatible with skin have allowed usage of ZnO as UV-blockers in sunscreen and other cosmetic products. ZnO has shown sizeable antibacterial drug activity and can strongly fight microorganisms. The ability of ZnO to encourage the generation of reactive oxygen species (ROS) has led to its application as an anticancer and antibacterial material (Condello et al., 2016). In addition, ZnO-based NSMs are effectively used in a drug delivery system in various diseases targeting some drugs to various tissues and cells. Another notable application of ZnO is in the field of sensing and imaging used to monitoring and track patient's health and be a suitable bio-imaging tool.

The ZnO NSMs possess a high isoelectric point of 9.5, suitable for absorption of lower isoelectric point materials such as proteins by the electrostatic interactions (Degen et al., 2000). The application potential of ZnO is well supported by its cost-effectiveness, lower toxicity, and low probability of interference with the major available pharmaceuticals compared to other metal oxide NSMs (Sahdev et al., 2013). The structural morphology of ZnO NSMs in various forms such as tubes, combs, and rods, has encouraged the use of ZnO for the immobilization of biological molecules in designing enzyme biosensors, immune-sensors, etc., (Dai et al., 2009). ZnO NSMs have also been acknowledged as important and versatile materials that play a key role in human life in the near future. In this review, a detailed understanding of the NSMs of ZnO, their synthesis, structural morphology, and applications in the field of biosensors are discussed with examples and illustrations.

2. Synthesis of ZnO nanostructured materials

The synthesis of ZnO NSMs has been reported using a variety of methods such as hydrothermal, sol-gel, chemical vapor deposition, precipitation in water, and mechano-chemical processes. Different techniques have been used to synthesize ZnO NSMs with different sizes, shapes, and structures as well as 1-D, 2-D, or 3-D NSMs. Among these, 1-D nanostructures make-up the largest group, which include structures such as rods, combs, tubes, ribbons, rings, needles, wires, and helices. The 2-D nanostructures are synthesized as nanoplates, sheets, and pellets, whereas flower-like, snowflake, urchin, and dandelion (dendrimers) particles have been obtained as 3-D structures. In this section, synthetic protocols of ZnO NSMs are discussed with representative examples.

2.1. Nanorods

The geometries of 1-D nanostructure are enormously attractive because they guide the charge carriers during conduction; nanorods are one such NSMs. Carbon fabric has proven to be an excellent tribological substrate for the growth of ZnO nanorods. Initially, a seed solution was prepared using zinc acetate dihydrate (0.11 g) and sodium hydroxide (0.04 g) dissolved in 250 mL of ethanol, the mixture was stirred for 30 min and aged for 24 h. Further, a growth solution was prepared using zinc nitrate hexahydrate (3.71 g) and hexamethylenetetramine (1.75 g) in 500 mL deionized (DI) water. In the seed solution, the treated carbon fabric was immersed for 10 min and dried at 100 °C. The process of dipping and drying was repeated three-times followed by dipping in the growth solution for 10 h at 90 °C. Thus synthesized ZnO nanorods were uniform and hexagonal wurtzite with a length of 500 nm having a diameter of 6 μm (Fei et al., 2018).

A three-step process for the growth of ZnO nanostructures on a patterned seed layer using chemical bath deposition was also proposed (Urgessa et al., 2018), which involved the deposition of seed layer, electron beam lithography (EBL) patterning of a poly(methyl methacrylate) (PMMA) mask, and finally the growth of nanorods. The ZnO seed layer was synthesized using $Zn(Ac)_2.H_2O$ dissolved in ethanol and agitated for 30 min at 30 °C. Mono-disperse nanoparticles were formed by adding poly(vinylpyrrolidone), which forms a shell around the nanoparticles. After allowing the reaction to proceed for 30 min, the solution was spin coated onto Si substrate five-times for 30 s each at 2000 rpm and finally annealed at 250 °C in flowing oxygen atmosphere. Further, for EBL patterning, a 50 nm thick layer of PMMA was coated onto the seed layer and baked at 180 °C for 2 min. Nanorods were then grown by dipping the seeded substrate in a 50 mM solution of $Zn(NO)_3.6H_2O$ and hexamine in 30 mL deionized (DI) water in a glass beaker kept in a water bath at 85 °C for 90 min. The pitch and pit diameters were used to control distribution and size of the resulting ZnO nanorods (Urgessa et al., 2013).

Qi et al. (2018) synthesized ZnO nanorods by titrating $Zn(Ac)_2.H_2O$ in NaOH under an electric field ranging between 0 and 0.5 kV cm^{-1} at 80 °C. The effect of the presence and absence of electric field on the morphology of ZnO NSMs was investigated, wherein it was observed that in the presence of a 0.5 kV cm^{-1} electric field, the synthesized nanorods were 2.0 μm long with a diameter of 40.0 nm, whereas, in the absence of an electric field, NSMs were rice-like grains having a size of around 40 nm. The synthetic process was simple involving the injected and base solutions. The injected solution was prepared by dissolving 5.95 g of $Zn(NO)_3.6H_2O$ in 10 mL of ethanol, which was transferred into the syringe. The base solution was prepared using 1.6 g NaOH in 200 mL DI water in a steel vessel connected to a high-voltage power supply, which served as the counter electrode. The needle connected to the syringe acted as an electrode to which an electric field was applied. Vertically aligned ZnO nanorods with controlled diameter and spacing were fabricated by combining EBL and chemical synthesis. The synthesized ZnO nanorod arrays had diameters ranging between 50 and 130 nm (Lamson et al., 2018).

2.2. Nanobelts

Considering different forms of NSMs, nanobelts have a rectangular cross section and have the morphology like a belt or a ribbon with the ratio of width to thickness of 5–10. Owing to this small thickness, these materials are promising for applications in sensing devices (Jali et al., 2018). Kaur et al. (2017) followed a carbothermal reduction for the synthesis of ZnO nanobelts. The synthesized nanobelts were used as a gas sensor that showed an excellent response at ambient temperature for H_2S and NO. Graphite and ZnO in the ratio 1:3 by weight were heated at 1050 °C in a furnace under argon atmosphere for 5 h. The furnace was cooled to room temperature and then the ZnO nanobelts were collected as spongy, cottony materials at the bottom of the furnace. Morphological investigations suggested the length and diameter of the nanobelts were in the range of 100–200 nm. Qu et al. (2012) fabricated porous ZnO nanobelts by a two-step process involving the preparation of a precursor and removing ligand and water molecules, by calcination to form the porous ZnO nanobelts. The arrangement of Zn and O atoms is usually not affected by removing water and small organic molecules. The heating process also provided the energy required for self-assembly oriented in the [0001] direction. This has resulted in the optimization of catalytic activity of ZnO nanobelts. Here, the reagent concentration was the key factor for controlling the morphology and size of the nanobelts.

Jang et al. (2010) reported the synthesis of non-porous and porous nanobelts, hierarchical and multipod NSMs using Zn-based hydroxide double salt (HDS) with dumb-bell shaped ZnO. The non-porous nanobelts were synthesized via a soft solution process using Na_2CO_3 as a dehydrating agent at 95 °C. `Further, it was observed that the porosity of ZnO nanobelts was affected by the intercalated H_2O molecules. Hence, the nanobelts were calcinated at 200–400 °C to obtain the

porous ZnO nanobelts. Hierarchical and flower-like structures were also obtained from the Zn-HDS by hydrothermal reaction at 230 and 150 °C using NaOH as a dehydrating agent.

2.3. Nanocombs

ZnO nanocombs and saws have the ordered structures and defined geometry. Because of this, they have attracted much interest to develop biosensors. The ZnO nanocomb structures have been fabricated using various techniques including carbothermal evaporation using graphene nanoplatelets and ZnO nanoparticles to make single and double-sided nanocombs assisted by oxygen at ambient temperature (Yildirim et al., 2015).

Mousavi et al. (2012) reported comb and saw-like NSMs fabricated by directly oxidizing Zn powder. The crystal structure was wurtzite comprised of nano and microstructures of comb and saw-shaped ZnO. Thermal evaporation method reported by Fan et al. (2012) enabled the growth of single crystals of nanocombs in the [0002] direction. In addition, temperature-dependent Raman spectra suggested that surface optical modes increased with a decrease in temperature. Further, Zhang and Bai (2011) reported the synthesis of macroscopic ZnO combs ranging from several millimeters to centimeters by the thermal evaporation using CuO as a catalyst.

2.4. Nano hierarchical

Hierarchical ZnO NSMs have proven to make exceptional sensors, and a survey of the literature reveals various methods of synthesizing these NSMs. The commonly used techniques are wet chemical, bio template, flame, and hydrothermal methods (Meng et al., 2017; Zhang et al., 2017; Li et al., 2016). Wang et al. (2018) proposed a method for the synthesis of 3-D cake-like ZnO NSMs via a solvothermal technique using DMF as a mediator. Further, as-prepared NSMs were deposited with Ag nanoparticles by the photochemical deposition. The synthesis was carried out at ambient temperature using a mixture of 20 mL DMF and 5 mL of water into which 1 mmol $ZnSO_4.7H_2O$ was added and stirred by adding 0.5 mmol NH_4BF_4. The final solution was sealed in Teflon-lined autoclave at 120 °C for 24 h, was cooled, centrifuged, and rinsed with water and ethanol; the product was dried at 70 °C.

Sun et al. (2014) reported a facile hydrothermal method for the controlled synthesis of ZnO nanoforests. Additionally, systematic investigations were performed to understand the individual as well as cooperative influence of ammonia and poly(ethylenimine) on the structure of nanoforests. The synthesis of nanoforests was carried out by drop casting ZnO seed solution onto the surface of pre-synthesized nanowire arrays followed by hydrothermal reaction. The concentrations of ammonia and poly(ethylenimine) were varied to control and fine-tune the growth of ZnO branches on the nanowire (NW) arrays. Several other methods of synthesizing ZnO NSMs are summarized in Table 1. Fig. 1 shows SEM images of ZnO NSMs synthesized with different methods and Fig. 2 shows the schematic synthesis of ZnO NSMs.

3. Bio-functionalization of ZnO

Fabrication of precise biosensors with surface functionalized nanostructured metal and metal oxides remain continues to challenge. Covalent and non-covalent interactions formed with different methodologies are used to functionalize NSMs, introducing different organic and functional groups enhancing the attachment of biomolecules through electrostatic interactions or specific bonds. Functionalization increases the stabilization and also reduces the agglomeration of metal nanoparticles. The interface between the inorganic and the organic matter has attracted much interest due to the improved and specific functions compared to pure organic and inorganic materials. Immobilization of biological recognition elements such as enzymes, protein receptors, probe molecules, cell receptors, etc, on the surface of the transducer, develops a bio-sensitive layer, thereby serving to capture the targeted analyte. Modifications of the NSMs are explored using many organic compounds including carboxylic acids, thiols, and amines, etc. Further, in the literature, one can find different modes of interaction of biomolecules with the metal surface of which few are discussed below.

High isoelectric point (IEP) of ZnO (pH 9.1) is helpful in the immobilization of biomolecules onto the surface of ZnO. Tak et al. (2014) synthesized flower-like ZnO NSMs onto platinized silicon substrates and investigated the interactions between single-stranded DNA and ZnO NSMs by cyclic voltammetry. The isoelectric point of ZnO was relatively high (IEP ~ 9.5) at pH 7.0 and it acted as a positively charged matrix onto which a negatively charged DNA with a lower isoelectric point (IEP ~ 4.2) was immobilized by the strong electrostatic attraction. The quantification of ss the-DNA was 5–240 ng μl^{-1} with a low detection limit of 5 ng μl^{-1}.

A similar mechanism was proposed by Ansari et al. (2009), where UV visible spectra showed a blue shift from 371 nm to 345 nm after immobilization of DNA, indicating electrostatic interaction between the positively charged ZnO NSMs and negatively charged DNA.

Kumar et al. (2019) investigated DNA binding potential of ZnO NSMs synthesized from the leaf extract of *Justicia wynaadensis*. The hyperchromic shift in absorbance showed the interaction between CT-DNA and ZnO nanoparticles, which has changed the DNA structure through the intercalated mode. Similar results were reported by Preedia et al. (2015). UV visible absorption spectra showed maximum absorption at 260 nm. With increasing concentration of ZnO, the absorbance of CT- DNA decreased at 260 nm with red shift, which signifies that π-π^*

Table 1
Summary of ZnO nanostructures and their synthesis techniques.

Structure of ZnO	Matrix used	Technique	Ref.
ZnO films	GaN layers	Hydrothermal	Ko et al. (2018)
ZnO crystals	Polycrystalline material	Chemical vapor transport	Fan et al. (2018)
ZnO nanoneedle array	Quartz crystal microbalance	Chemical deposition method	Cha et al. (2018)
ZnO thin films/nanorods	Si	Magnetron sputtering	Nandi et al. (2017a)
ZnO nanowires	Optical fiber surface	Hydrothermal process with an efficient UV irradiation	Gong et al. (2017)
ZnO nanorods and nanowires	Au–Ag alloy	UV pulsed laser deposition	Dikovska et al. (2017)
ZnO films	MgO	Pulsedlaser deposition	Perrièrea et al. (2018)
ZnO clusters	Graphite	Hydrothermal synthesis	Rodrigues et al. (2018)
TiO_2 coated ZnO nanorods	–	Chemical vapor deposition process followed by nano-cluster deposition	Eadi et al. (2018)
ZnO nanofibers	Teflon substrates	Chemical bath deposition	Farhat et al. (2016)
ZnO nanowires	Zinc foils	Thermal oxidization	Wu et al. (2017)
ZnO nanorods	Pyrolytic graphite	Spray pyrolysis	Hossein-Babaei (2017)
Cu doped ZnO thin film	–	Sol-Gel method	Asikuzun et al. (2018)
ZnO nanorods	Glass substrates	Microwave plasma-assisted thermal evaporation	Thongsuksai et al. (2018)
Hierarchical nanoarchitectures	ZnO nanowires	Thermal oxidation combines lattice/grain/surface ionic diffusion	Sombrio et al. (2017)

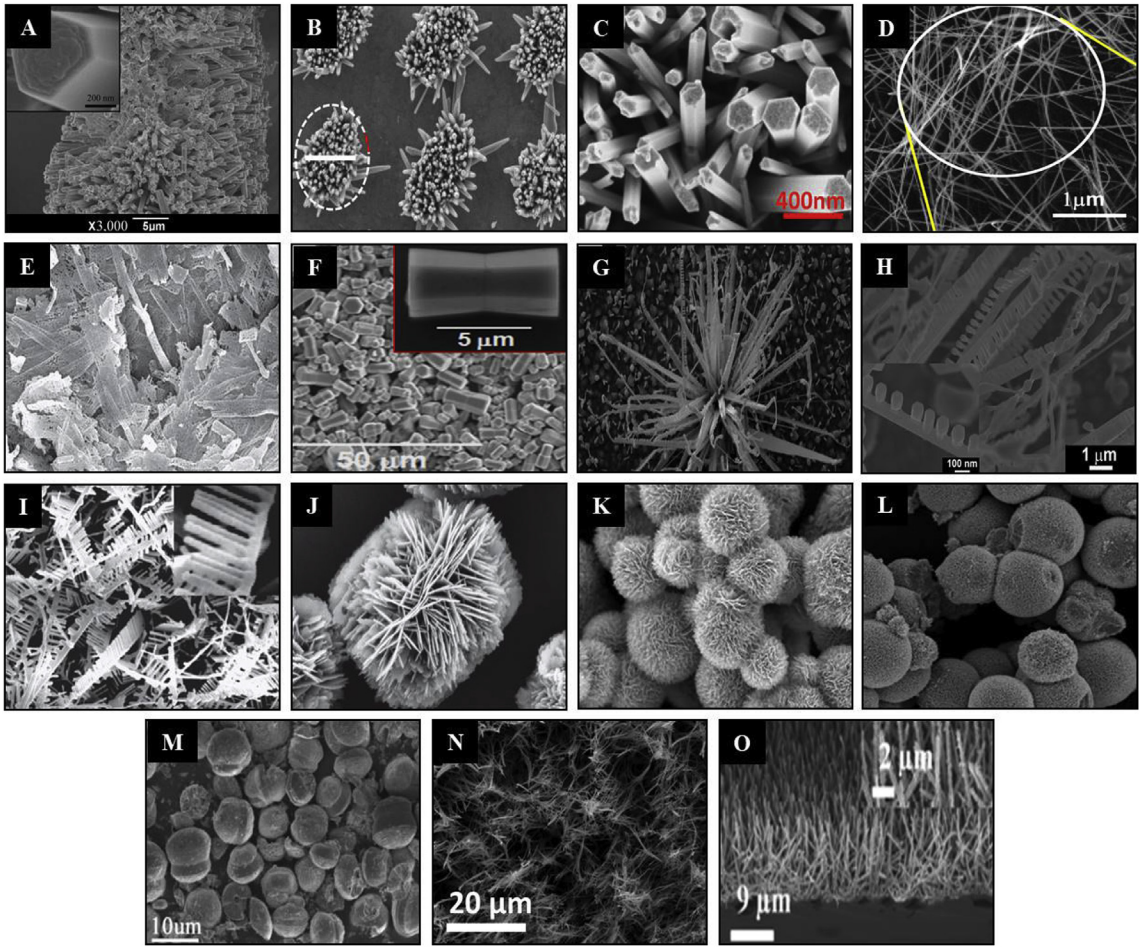

Fig. 1. SEM images of nanorods (A–C) [ref. Fei et al. (2018); Urgessa et al. (2018); Jali et al. (2018); nanobelts (D–F) [ref. Kaur et al., 2017; Qu et al., 2012; Jang et al., 2010]; Nanocombs (G–I) [ref. Yildirim et al., 2015; Fan et al., 2012]; hierarchical (J–O); J) FESEM image of nanosheets [ref. Qu et al., 2018], K) SEM image of porous ZnO microflowers [ref. Song et al., 2018.] L) Non-porous ZnO microflowers [ref. Song et al., 2018] M) SEM image of 3D cake-like ZnO/Ag microstructures [Wang et al., 2018] N) FESEM images of deposited ZnO NWs [ref. Ebrahimi et al., 2018.] O) SEM image of ZnO nanoforests [ref. Sun et al., 2014.] synthesized by different methods.

stacking interaction between ZnO nanoparticles and the base pair of DNA reveals the binding of DNA with the ZnO nanoparticles via intercalating mode.

ZnO NSMs having a high surface area to volume ratio, the tendency to aggregate and high electron mobility would provide a favorable situation for enzyme immobilization. Purified chitinase from Vigna mungo and N-acetyl glucosaminidase (NAGase) from Canavalia ensiformis were immobilized onto polyurethane (PU)/zinc oxide nanoparticles (Preety and Hoooda, 2018). Adsorption of enzyme has shifted the peak for nano ZnO from 712 to 621 cm^{-1}. However, retention of peaks for the nano ZnO and the disappearance of characteristic PU peaks clearly indicated that enzymes were simply absorbed onto the nano ZnO surface, but were covalently linked to the PU support. Fabrication of high-sensitive glucose sensors based on ZnO nanorods integrated with ZnO-based FETs, patterned growth of ZnO nanorods and enzyme immobilization on their surfaces were studied by Ogata et al. (2010). Here, covalent and electrostatic bonding method was used for the immobilization of glucose oxidase onto the surface of ZnO nanorods.

Wang et al. (2015c) investigated protein adsorption onto the surface of ZnO nanostructures with different topologies. Kinetics of adsorption of mono-proteins such as fibrinogen and bovine serum albumin (BSA) on the surfaces of ZnO nanoparticles, sheets, beams, and rods have been discussed. A comparison between the adsorption of BSA and fibrinogen suggested that fibrinogen requires a longer time to attain equilibrium than BSA. This was explained based on the isoelectric points of ZnO (IEP ~ 9.5), BSA (IEP ~4.6), and fibrinogen (IEP ~ 5.5). In phosphate buffer solution of pH 7.4, because ZnO is positively charged, less electrostatic repulsion is observed for BSA, which has a higher negative charge due to its lower isoelectric point compared to that of fibrinogen. Further, fibrinogen has a slightly higher affinity for hydrophobic surface, but the mobility of fibrinogen (340 kDa) is lower as its molecular weight is higher than BSA (66 kDa). Hence, more of BSA was adsorbed onto the surface of ZnO NSMs. It was concluded that ZnO nanorods had more binding sites than the other ZnO NSMs, which provided more prospects for protein interactions with the surface.

Ansari et al. (2010) proposed a method for the deposition of nano ZnO onto the surface of an indium tin oxide glass plate immobilized with BSA and rabbit immunoglobulin antibodies (r-IgGs) for the detection of ochratoxin-A. FTIR spectroscopic investigations suggested that r-IgGs amide groups connected to Zn–O nanoparticles have shifted the diffusion band at 3441 cm^{-1} due to the O–H stretching towards 3214 cm^{-1} as a result of –CONH stretching vibration. Hence, it was concluded that r-IgGs macromolecule was bonded to Zn–O–Zn network by the –H bonding and electrostatic attractions. Further, the literature suggests that interaction of ZnO and biomolecules has been widely studied and it would not be possible to discuss these data in this review. Fig. 3 shows a schematic representation of the fabrication of ZnO NSMs biosensors.

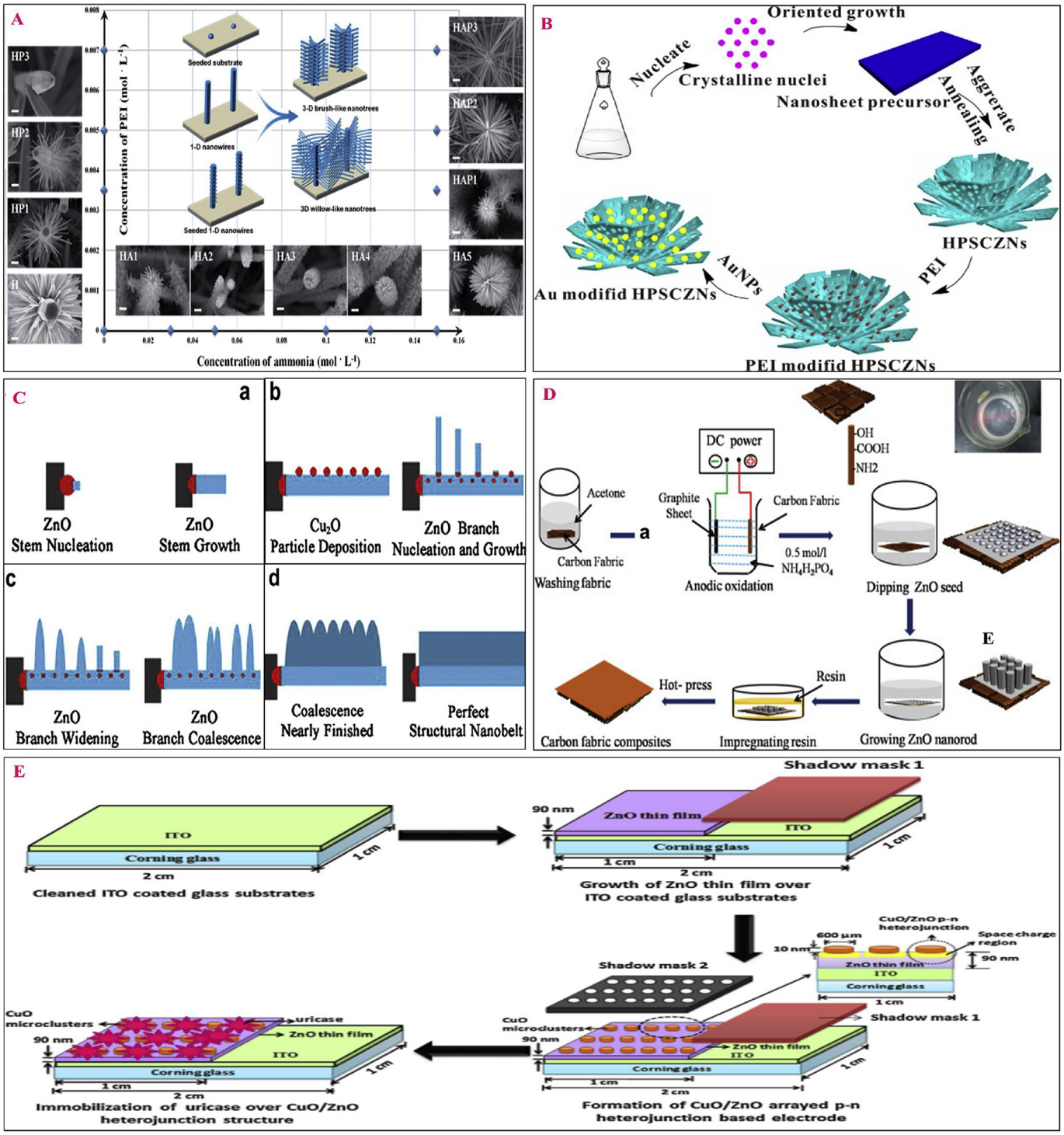

Fig. 2. A) Morphology illustration and size evolutions of ZnO nanobranches onto preformed ZnO nanowire arrays to form the ZnO nanoforest by altering ammonia and PEI concentrations of the nutrient solution during the branch growth process (Sun et al., 2014); B) Schematic illustration of the formation process of the Au-modified HPSCZNs (Meng et al., 2017); C) The model for the nanocombs growing into nanobelts. (a) ZnO stem nucleation and growth; (b) ZnO branch nucleation and growth; (c) ZnO branch widening and coalescence (d) Resulting perfectly structural nanobelts (Zhang and Bai, 2011); D); Schematic of growing aligned ZnO nanorods on carbon fabric and the process used to prepare the composite (Fei et al., 2018); E) Schematic representation of fabrication process of CuO/ZnO arrayed p-n heterojunction bioelectrode (Jindal et al., 2017).

4. Applications of ZnO as a biosensor

The immobilization of biomolecules on the nanostructure to be used as a platform for biosensors is mainly dependent on the shape, size, and properties of the nanostructure. Advances in the field of ZnO crystal growth have allowed the synthesis of about 10-types of ZnO NSMs, including thin films, nanorods, quantum dots, nanoparticles, nanowires, and others. Various inherited properties of ZnO nanoparticles have allowed the successful immobilization of different types of biomolecules on their surfaces. Nanostructures such as nanowires (Politi et al., 2015a, 2015b), nanorods (Wu et al., 2015; Wang et al., 2014), nanoparticles (Picciolini et al., 2015; Huang et al., 2015), quantum dots

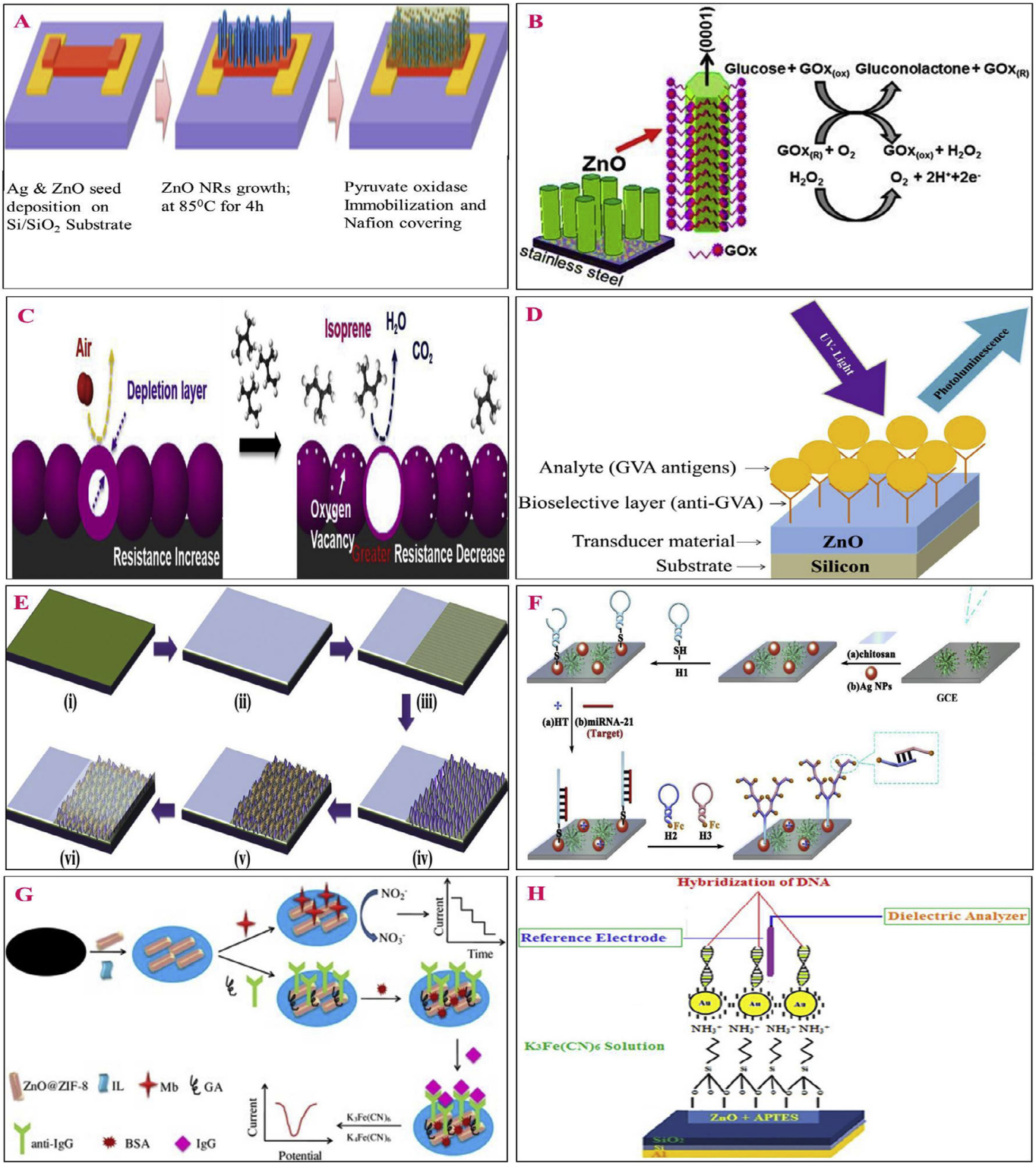

Fig. 3. A) Schematic showing FET biosensor fabrication (Ahmad et al., 2017b); B) Schematic representation of GOx/ZnO/SS sensor and electrochemical reactions (Rodrigues et al., 2018); C) A schematic of the sensing mechanism of ZnO QDs in air and isoprene (Park et al., 2019); D) The scheme of the PL based immunosensor (Tereshchenko et al., 2017); E) Schematic illustration of the fabrication process of uric acid biosensor. (i) Cleaning of Si substrate; (ii) Silver deposition by sputter; (iii) ZnO seed layer deposition by sputter; (iv) growth of ZnO NSs; (v) Uricase enzyme immobilization (vi) Nafion covering to protect enzyme (Ahmad et al., 2015); F); Fabrication process of developed biosensor for miRNA-21 detection (Zhang et al., 2019); G) Illustration to prepare ZnO@ZIF-8/IL/Mb-CPE and ZnO@ZIF-8/IL/GA/anti-IgG/BSA/IgG-CPE. (Dong, 2017); H) Scheme of the probe DNA-ZnO/APTES/Au electrode (Mohammed et al., 2017).

(Gu et al., 2011), thin films (Iyer et al., 2014; Shukl et al., 2015), and some low-dimensional nanostructures (Tak et al., 2014; Xie et al., 2015; Liu et al., 2014) have been extensively reported in bio-sensing applications. In addition, the analyte most commonly used as a detecting material can be classified as: molecules having a lower molecular weight: dopamine, uric acid, urea, and riboflavin; proteins: BSA,

HAS, immunoglobulin, streptavidin; Nucleic acid: RNA and DNA; cells: cancer cells, infectious cells, bacteria, and viruses.

4.1. Biosensors for small molecules

Rahmanian et al. (2018) proposed an impedimetric biosensor for the detection of urea, fabricated using DC-sputtered nano ZnO on a TiO_2 thin film. On the surface of fluorinated tin oxide previously covered with TiO_2, a 3-D hierarchical ZnO NSMs was fabricated by DC sputtering of ZnO using poly(vinyl alcohol) as an omissible polymer (nano-ZnO/PVA/TiO_2/FTO). Further, the omission by annealing produced a porous surface suitable for urease immobilization. The proposed biosensor showed a good response time with good enzyme activity over a longer period. The electrochemical detection of urea based on fluorine-doped tin oxide/polyamide6/polypyrrole/ZnO/urease electrode was proposed by Migliorini et al. (2018). The results suggested that electrospun nanofiber-based electrodes could be an excellent platform for the analysis of dairy products.

Uric acid, a key component of blood serum and urine, is a nitrogenous material and a primary product, obtained due to the metabolic breakdown of purine nucleotides. The permissible range for men and women is 0.214–0.506 mM and 0.137–0.393 mM, respectively. Elevated or decreased levels of uric acid lead to many physiological disorders in humans, such as kidney diseases, gout in the joints, multiple sclerosis, and arthritis (Barrett et al., 2010). Jindal et al. (2017) fabricated a ZnO thin film and CuO micro-cluster for the immobilization of uricase for the detection of uric acid.

Cyclic voltammetric investigations were performed to investigate the performance of the fabricated p-n junction-based biosensor. The built-in electric field facilitated charge transport, which in turn decreased the potential required to sense the uric acid. The uricase/CuO/ZnO/indium tin oxide/glass bio-electrode was fabricated by drop-casting a solution of freshly prepared uricase onto the surface of a CuO/ZnO/ITO/glass electrode. Strong electrostatic adsorption of uricase was observed due to the higher isoelectric point of ZnO and CuO. The ZnO nanosheets grew directly onto the surface of Ag/Si, prepared by sputtering Ag on the surface of Si, which was reported as a substrate for an alternate sensitive method for the detection of uric acid (Ahmada et al., 2015). The electrode was fabricated by sputtering a thin ZnO seed layer of about 50 nm thick on the surface of Ag/Si electrode and then ZnO nanosheets were grown using a low-temperature aqueous route. The surface was converted to be hydrophilic prior to immobilization of the uricase enzyme by dipping in a phosphate buffer solution and then dried under nitrogen gas atmosphere. Electrode fouling and leaching of enzyme were eliminated by drop casting 5 μL of Nafion solution on the fabricated electrode. Cyclic voltammetric investigations suggested that conductivity of ZnO nanosheets played a crucial role in producing well-defined peaks, while H_2O_2 produced during the reaction catalyzed by uricase was oxidized to generate the electrons through the electrode, which enhanced the current response.

Riboflavin or vitamin B2 is very important in converting carbohydrates, proteins, and fats into energy and also supports the body during the stress of daily life (Tan et al., 2012). A glassy carbon electrode (GCE) modified with ZnO and manganese hexacyanoferrate (MnHCNF) was demonstrated to detect riboflavin (Selvarajan et al., 2018). The electrode was easily prepared by drop casting and drying the ZnO onto GCE surface on which MnHCNF was then deposited. The cyclic voltammogram obtained for 1.0 mM riboflavin showed that the electrode process was reversible. Gao et al. (2018) used ZnO nanowire arrays along with graphene and graphene foam to detect folic acid. The graphene foam was synthesized by a chemical vapor deposition method and the nanowires were grown on the graphene foam using a hydrothermal method. Further graphene was deposited on the nanowires to form Gr/ZnO NWAs/GF NSMs.

4.2. Use of ZnO nanostructures as biosensors for detection of infectious diseases

4.2.1. Detection of malaria

An electrochemical immunosensor based on copper-doped ZnO nanofibers was used for detection of PfHRp-II. Nanofibers were coated onto the surface of GCE, which was synthesized by an electrospinning technique and functionalized with mercaptopropyl phosphonic acid. The PfHRP-II-specific monoclonal antibodies were absorbed on the electrode surface, which improved the impedance response with a sensitivity of 28.5 kΩ/(g/mL)/cm^2. Chemiresistive biosensors based on multi-walled carbon nanotubes and ZnO nanofibers for the detection of HRP-II were demonstrated. Advantage of the proposed method was the use of low-cost materials and the ability for on-site diagnosis in a low resource setting by using a thin film of poly(ethylene terephthalate) instead of a conventional electrode. Anamide bond was formed at the carboxyl terminal of ZnO nanofibers for covalent conjugation of antibodies specific to HRP-II. The sensor operation was based on a change in the resistance of electrode due to binding of HRP-II, if present in the solution, to the antibody at the electrode surface (Paul et al., 2016; Paul et al., 2017).

4.2.2. Detection of dengue virus

Fluorine-doped tin oxide (FTO) glass plates modified with ZnO/platinum-palladium (ZnO/Pt–Pd) have been proposed as electrochemical genosensors for the determination of the DNA sequence of dengue virus using methylene blue as an intercalating agent (Singhal et al., 2017). The sensor was developed by immobilizing the probe DNA onto a ZnO/Pt–Pd -modified FTO electrode surface. Interaction between methylene blue and free guanine of ssDNA reduced the current, which was used to detect the hybridization between the probe DNA and the targeted DNA.

4.2.3. Detection of bacterial meningitis

A hydrothermal method to synthesize flower-like ZnO NSMs on platinized silicon substrates was proposed for immobilization of ss-thiolated DNA probe of Neisseria meningitides. Morphological investigations of ZnO NSMs suggested that it consisted of ZnO nanorods, oriented radially with an average diameter of 100 nm and a length of 2.5 μm with the tips of the rods having a hexagonal shape. The detection of targeted DNA using the biosensor was highly selective with a sensitivity of 5–240 ng/μL and sensitivity of 168.64 μg/ng-μL. Impedimetric investigations were also promising to detect meningitis over the linear range of 10–200 ng/μL with a sensitivity of 18.56 Ω ng/μL (Tak et al., 2014).

Nickel-doped ZnO thin film electrodes for electrochemical detection of meningitis were proposed by Tak et al. (2017) and experiments were performed by immobilizing oligonucleotide sequences of DNA onto the surface of Ni-doped ZnO/ITO electrode. Methylene blue-mediated buffer solution was used in differential voltammetry that showed a good response in the linear range of 5 ng/μL - 200 ng/μL with a detection limit of 5.0 ng/μL.

4.2.4. Detection of grapevine virus

Optical biosensors for the determination of grapevine virus based on ZnO thin films deposited using atomic layer deposition were proposed (Tereshchenko et al., 2017). The surface structural properties of the fabricated ZnO thin films were favorable for the immobilization of antibodies against grapevine virus-antigens, thus providing a suitable platform for detecting grapevine virus-antigens. Evaluation of charges and behavior of the corresponding luminescence band were used to detect grapevine virus-antigens in the linear range of 1.0 pg/mL - 10 ng/mL. Optical properties of the fabricated sensor were investigated by recording absorbance spectra in the range of 250–600 nm, suggesting that anti-grapevine virus antibodies lacked any optical activity in that range. Grapevine virus antigens were detected by measuring

changes in photoluminescence (PL) band behavior; however, a new PL band appeared in the region 400–500 nm due to Zn–S bonding.

4.3. Cancer biomarker detection

Early detection of cancer in patients is an on-going challenge, which can provide a suitable starting point for developing new strategies for the treatment of tumors. Low-cost, rapid, and label-free detection, as well as portability, are some of the hurdles that need to be overcome. In the United States, ovarian cancer is the fifth most common cause of death in women. There are various markers associated with ovarian cancer. One of them is mucin 16, which is found on the ovarian cancer cells, consisting of high molecular weight glycoprotein and its antigen circulating in the blood. About 90% of women suffering from ovarian cancer are found positive towards mucin 16. An electrochemical method based on ZnO nanorod-Au nanoparticle structures was used for early detection of mucin 16, wherein hydrothermal synthesis was used to develop ZnO nanorods onto the surface of gold and silver surfaces for use as a working electrode and followed by depositing Au nanoparticles by sputtering. This electrode was further loaded with anti-mucin 16 antibodies. The Au nanoparticles on ZnO nanorods interacted with glutaraldehyde and cystamine in the antibodies to form a strong bond.

Immunosensor showed good stability and reproducibility with a limit of detection of 2.5 ng/μL and proved promising in clinical applications (Gasparotto et al., 2017). Fig. 4 shows a schematic representation of the fabrication of ZnO NSMs biosensor for infectious diseases. A photo-electrochemical immunosensor based on ZnO nanorods was also proposed to detect nucleoside diphosphatase kinase-A (NDPK-A) (Liu et al., 2017). It is a protein that suppresses metastasis and is also a biomarker for a wide range of cancer cells. ZnO nanorods sensitized with Mn^{2+} and CdS nanoparticles were used to immobilize anti-NDPK-A antibodies.

The study further suggested that upon irradiation with the visible light, the photocurrent increased in the order of bare FTO < ZnO nanorods grown on FTO < CdS: Mn co-sensitized ZnO nanorods. However, after the immobilization of anti-NDPK-A antibodies, the photocurrent response decreased due to the large spatial dimension of NDPK-A, which hinders the diffusion of H_2O onto electrode surface to generate holes, thereby reducing the light-absorbing area of ZnO and CdS:Mn. The electrode showed a low detection limit of 0.3 pg/mL and provided a more accurate and reliable operating environment for the detection of NDPK-A.

4.4. ZnO biosensors based on field effect transistors

Field effected transistor (FET)-based biosensors have recently attracted much interest for bio-molecule detection due to their advantageous properties such as fast electrical detection, easy to move from one place to another, label-free, low-cost for mass production and sensor as well as measurement systems are compatible to be integrated into a single chip (Sarkar et al., 2014). FET-based biosensors work on the principle that enables the detection of a biomolecule by producing the surface potential on the surface of a transducer upon biological interaction contribute to the modulation of the current flow inside the channel, located between two regions, which are drain and source.

Specific biological receptor such as DNA, RNA, aptamers or antibodies are mobilized onto the surface of a transducer through covalent binding with suitable chemical linkers are required for specific detection of biomolecules. Zong and Zhu (2018) reported glucose biosensor for using ZnO nanorods based on FET. Between the source and drain microelectrodes semiconducting ZnO nanorods were grown by using the AC electric-field assisted hydrothermal growth and serve as the conductive channel of FET. The fabricated sensor showed a tiny sensing area of 180 μm^2 with a high sensitivity of 1.6 mA/(μM-cm^2) and a detection limit of 1 μM.

Ahmad et al. (2017a) proposed a method for growing ZnO nanorods on the substrate via a low-temperature aqueous route. Further, ZnO nanorods were functionalized with pyruvate oxidase to detect phosphate. Fabricated FTE under optimum conditions showed a high sensitivity of 80.57 $\mu A\, mM^{-1}\, cm^{-2}$ in a wide-linear range of 0.1 μM–7.0 μM. Encouraging results suggested that this approach presents a promising method to be used for field measurements to detect phosphate. Fathil et al. (2017) presented substrate-gate coupling in FET-based biosensor for the detection of cardiac troponin I (cTnI) biomarker. Immobilization of cardiac troponin I monoclonal antibody (MAb-cTnI) as a bio-receptor for capturing cTnI biomarker was via covalent binding. The biosensor exhibited a high sensitivity with a detection limit of 3.24 pg/ml.

4.5. Biosensors based on morphology of ZnO

Due to high surface-to-volume ratio quantum dots (QDs) show unique features, since surface atoms affect catalytic, electronic, optical, magnetic properties of the nanomaterials (Bajorowicz et al., 2018). QDs possess unique properties, such as long-time of radiance emission, high quantum yield (QY), narrow emission and broad absorption spectra. Absorption range of QDs can be easily tuned by adjusting their size due to their unique size and shape-dependent optical properties (Li et al., 2013). Park et al. (2019) reported the quantum-size effect on the sensing properties of ZnO nanoparticles for the detection of isoprene. ZnO QDs exhibited excellent sensing performance to 1 ppm of isoprene. The higher sensing, rapid response, and lower optimal working temperature of ZnO QDs may be attributed to increase in oxygen vacancies, band gap, and specific surface area owing to the small size effect.

Hosseinzadeh et al. (2016) studied the interaction of insulin with ZnO QDs and demonstrated how ZnO QDs alter the insulin structure. The investigations performed for thermal aggregation suggested that aggregation of insulin in the presence of ZnO QDs occurs in a short lag phase with the fast aggregation rate. Presence of ZnO QDs in the vicinity of insulin could change the structure of insulin. Hence, suitable surface functionalization of these QDs is necessary for applications such as in bio-imaging.

The tetrapod-shaped ZnO nanostructures are not something new to the community. Recently, Mishra and Adelung (2018) have published a review on ZnO tetrapods materials for functional applications. Lupang et al. (2009) prepared transferable ZnO tetrapods grown by aqueous solution method that was fabricated and its UV as well as gas sensing properties were investigated. When illuminated with the UV light, the sensor showed a decrease in resistance due to desorption of chemi-adsorbed oxygen from the surface and an increase in charge carrier density due to electron-hole pair generation. From the literature, it can be observed that ZnO tetrapods have been studied extensively in gas sensing as well as in UV sensors, field emission, antibacterial coatings, and piezoelectric power generation on the horizon. Therefore, ZnO tetrapod devices are likely to remain an active area of research for many years to come.

Rodrigues et al. (2018) developed nano-columnar ZnO film as a glucose biosensor. Vertically aligned ZnO nano-columns of ~80 μm wide and ~1 μm long oriented in the (0001) direction were functionalized with glucose oxidase enzyme. Higher sensitivity in a linear concentration range, 1.5 mM–16 mM was observed and immobilization of glucose oxidase occurred via hydroxyl groups in the presence of covalent bond interactions.

ZnO nanowires are promising piezoelectric transducers used to develop bio-molecular detection systems. Galdamez et al. (2019) demonstrated the fabrication of ZnO nanowires using VLS technique as an optical biosensor for detecting thiolated oligonucleotide probe labelled by cy5. Two different morphologies of nanowires based on orientation (i.e., random and straight) were developed and functionalized to study interaction with DNA. Electromagnetic and chemical enhancement for random-standing nanowires increased the surface enhanced Raman spectral (SERS) signals. Better surface modification after interaction

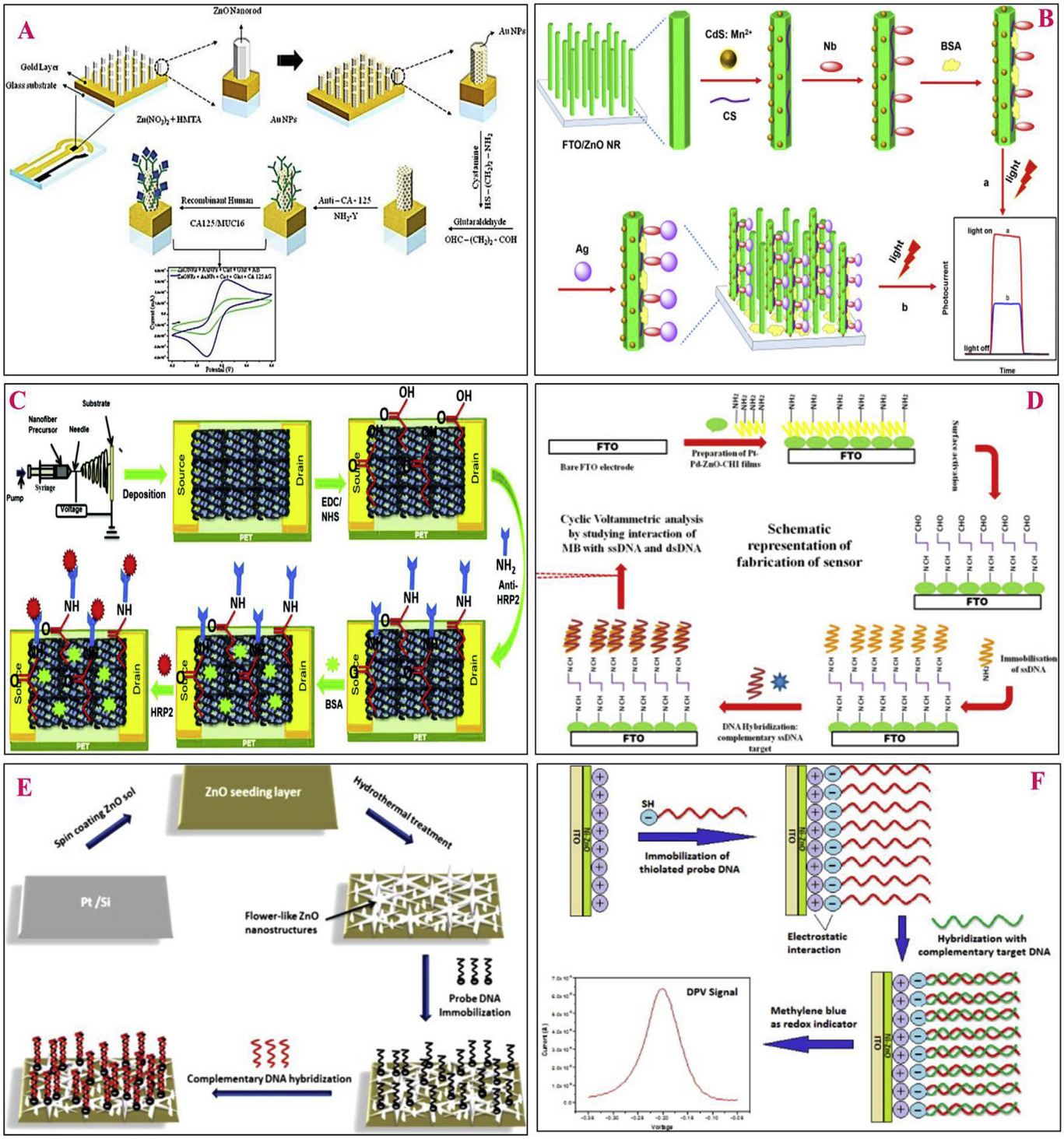

Fig. 4. A) Fabrication of ZnO NRs-Au NPs nanohybrids biosensor for CA-125 detection (Gasparotto et al., 2017); B) Schematic representation of construction of the PEC immunosensor (Liu et al., 2017); C) Schematic representation of fabrication of flexible chemiresistive biosensor for HRP2 malaria biomarker (Paul et al., 2017); D) Schematic representation of the fabrication of the sensor of the hybridization of the target DENV DNA (Singhal et al., 2017); E) Schematic representation of the fabrication of DNA bioelectrode (Tak et al., 2014); F) Schematic representation of the sensing mechanism for SH labelled probe DNA immobilized on Ni–ZnO/ITO electrode (Tak et al., 2017).

with DNA was observed for zig-zag orientation of ZnO nanowires, thereby opening a new gateway for developing optical biosensors.

Fung et al. (2017) used the flexographic printing technique with ZnO nanowires for an electrochemical biosensor of glucose. Flexographic printing technique was low-cost mass production and ultra-high output due to roll-to-roll nature of the technique, which is advantageous in developing technologies meeting the marked demands of bio-sensors. Neveling et al. (2014) studied nanoforce ZnO nanowire-array biosensor for detection and quantification of immunoglobulins. On the surface of ZnO nanowire with a self-assembled monolayer of 3-mercaptopropanoic acid was covalently linked with lysozyme and its response was linear with antibody concentration, 50 ng/ml - 1 μg/ml range with a detection limit of 102.76 ng antibodies/ml.

ZnO nanorods due to their advantageous properties of large surface-

Table 2
Summary of ZnO nanostructured materials used as a sensor for the detection of pharmaceutical drugs.

Electrode material	Analyte	Technique	LOD (nM)	Linear range (nM)	references
ZnO nanoparticles nano-silica composite	Atorvastatin	DPV	0.70	$2.5 – 6.5 \times 10^5$	Bukkitgar et al. (2018b)
ZnO/CNTs nanocomposite/ionic liquid/CPE	Noradrenaline	SWV	20	$50–4.5 \times 10^5$	Pahlavan et al. (2014)
ZnO/CNTs nanocomposite/catechol derivative modified electrode	Amoxicillin	SWV	500	$1000–9.5 \times 10^5$	Karimi-Maleh et al. (2014)
ZnO/CNTs nanocomposite/catechol derivative modified electrode	Glutathione	SWV	0.8	$2.0 – 7.2 \times 10^5$	Karimi-Maleh et al. (2014)
1-methyl-3-octylimidazolium tetra-fluoroborate and ZnO/CNTs nanocomposite	Raloxifene	DPV	40.0	$80–4.0 \times 10^5$	Cheraghi et al. (2017)
ZnO nanoparticle/1-butyl-3- methylimidazolium tetrafluoroborate/CPE	Doxorubicin	SWV	9.0	$70–5.0 \times 10^5$	Alavi-Tabari et al. (2018)
ZnO nanoparticle/1-butyl-3- methylimidazolium tetrafluoroborate/CPE	Dasatinib	SWV	0.5	$1000–12.0 \times 10^5$	Alavi-Tabari et al. (2018)
5% Barium-doped zinc oxide nanoparticle/GCE	Nimesulide	DPV	1.794	1.0×10^4–100	Bukkitgar et al. (2016b)
5% Barium-doped zinc oxide nanoparticle/GCE	Mefenamic acid	DPV	6.02	$500–10.0 \times 10^3$	Bukkitgar et al. (2015)

*DPV: Differential pulse voltammetry; SWV: Square wave voltammetry; GCE: Glassy carbon electrode; CPE: Carbon Paste electrode.

to-volume ratio and easy growth methods have attracted researchers in recent years. Tariq et al. (2018) fabricated ZnO nanorods grown by hydrothermal method for glucose detection using photolithography. The electrode showed good sensitivity (22.7 $\mu A cm^{-1}$ mM^{-1}). Increasing the pH of buffer solution and the length of nanorods increased the immobilization of glucose oxidase.

4.6. Metal oxide modified ZnO biosensors

Enhanced optical properties of NSMs coupled with metal oxide produce nano-hybrid materials enabled a new platform for both therapeutics and diagnosis applications (Li et al., 2015). Transition metal oxides such as $NiWO_4$ TiO_2, Fe_2O_3, and CuO, etc. can be used to form nanocomposite to catalyze analyte targeted. Zhou et al. (2014) proposed a non-enzymatic glucose biosensor using the electrospinning method to deposit ZnO–CuO hierarchical nano-composites on fluorine-doped tin oxide for detection of glucose. The electrode showed improved sensitivity of 3066 $\mu A mM^{-1} cm^{-2}$ and a detection limit of 0.21 μM.

Jung et al. (2018) developed a non-enzymatic FTE-based glucose biosensor. The ZnO nanorods grown between the source and drain were modified with NiO quantum dots by sputtering. The developed sensor showed a wide linear dynamic range of 0.001–10 mM and 10–50 mM with a high sensitivity of 13.14 $\mu A cm^{-2}$ mM^{-1} and 7.31 $\mu A cm^{-2}$ mM^{-1}, respectively. The system was used for a human whole blood sample and serum sample analysis. Ahmad et al. (2017b) reported a FET-based vertically oriented-based non-enzymatic glucose sensor. ZnO nanorods were modified with Fe_2O_3, which enhanced the performance of biosensor compared to ZnO-based non-enzymatic glucose sensors. Enhancement of this biosensor was attributed to excellent electro-catalytic nature of Fe_2O_3. In the linear range up to 18 mM, the fabricated sensor showed excellent catalytic activity with a detection limit of 12 μM. The sensor was used to detect glucose in freshly drawn mouse whole blood and serum samples, suggesting practical applicability of FET sensor in real sample analysis.

In addition to the above findings, many other metal oxide-modified ZnO nanostructures have been used as biosensors. Designing of a sensor consisting of multifunctional and NSMs would be easier with attractive properties of metal oxide-modified ZnO NSM-based biosensors. Utilization of such nano-hybrids in bio-sensing would revolutionize the diagnostic as well as environmental samples.

4.7. ZnO-carbon nanotube biosensors

Extraordinary properties of carbon nanotubes have outstanding opportunities for developing new technologies. When ZnO and carbon nanotubes (ZnO-CNT) are combined, exceptional properties can be generated that are not otherwise found individually. Recently, researchers have utilized these hybrids to develop sensors. ZnO-CNTs have been widely used as humid sensors (Dai et al., 2019), energy storage materials (Sankapal et al., 2016), opto-electro-mechanical response (Nandi et al., 2017), batteries (Ji et al., 2018), bone tissue engineering (Shrestha et al., 2017), photocatalyst (Fernandes et al., 2019), etc.

Karimi-Maleh et al. (2014) proposed a method to determine glutathione and amoxicilline in biological and pharmaceutical samples. Carbon paste electrode was modified with 8,9-dihydroxy-7-methyl-12H-benzothiazolo[2,3-b]quinazolin-12-one (DMBQ) and ZnO-CNTs. The square wave voltammetric investigation suggested the linearity range of 0.002–720 and 1.0–950 μM, respectively with detection limits of 0.0008 and 0.5 μM, respectively for glutathione and amoxicillin. Further, the electrode was applied for real sample analysis, demonstrating higher selectivity in the mixture of glutathione and amoxicillin. Moyo et al. (2015) used ZnO multi-walled carbon nanotubes (ZnO-MWCNT) for electro-oxidation of triclosan using combination electrochemical methods in a buffer solution of pH 7.0. The fabricated electrode showed an excellent response for triclosan in the linear range 1.5 $\mu g L^{-1}$ to 2.0 $mg L^{-1}$ with a detection limit of 1.3 $\mu g L^{-1}$.

4.8. Determination of pharmaceutical drugs

Detection of pharmaceuticals at low concentrations with lesser time is of high priority research. Literature suggests the application of various forms of ZnO NSMs for analyte detection. Low-level detection of drugs helps to monitor permissible amount of drugs in the human body. Methods reported in the literature are summarized in Table 2.

5. Summary and conclusions

The unique properties such as nontoxicity, piezoelectricity, biocompatibility, good conductivity, and large specific surface area have widened sensing applications of ZnO NSMs. New applications are being invented with advancements in nanotechnology that utilize ZnO NSMs for biomedical applications. In the present scenario, various forms of ZnO nanostructures can be synthesized by simple and cost-effective methods. Further, ZnO NSMs have shown different mechanisms of interaction with biomolecules, resulting in improved sensing ability. Addressing all research results is a formidable task and hence, the effort is made to discuss the synthesis of different nanostructures of ZnO, their mechanism of interaction with biomolecules as well as their applications as biosensors, considering smaller molecular weight compounds, detection of infectious diseases and pharmaceutical compounds.

6. Future prospects

ZnO surface of various morphology has been used for binding molecules and biomolecules for the detection of a respective analyte in configuration with different methods such as ion-sensitive field effect transistors, piezoelectric devices, electrochemical transducers, field effect transistors, and optical devices. The potential shown by FETs studies suggests that FETs will replace electrochemical detection as the choice for miniaturized biosensor applications. ZnO nanostructures-

based platforms in the future can provide nanosensor/nanodevices for monitoring multiple health parameters outside central labs. Technical application of ZnO biosensor requires growing ZnO NSMs on electrode surface in a repeatable and uniform manner. Fabricating these structures is advantageous for immobilization of analytes such as metabolites, DNA, and cancer markers, leading to alternate methods for clinical diagnosis leading to fabrication of feasible commercial biosensor and point of care measurement. Even though several fabrication procedures are already available the challenge is to mass production of well-controlled dimension and morphology 1D ZnO. Reproducibility of the fabricated biosensor is another concern need to be addressed that would help in the development of miniature devices for point of care diagnosis. Commercialization and real application in biosensor and healthcare field are way far and need much knowledge of the interaction of ZnO with biomolecules system. Lastly working of these devices in the biological pH needs to be extensively studied. This would be a much big milestone in areas of diagnostics and disease control.

Authors statement

All the authors of the manuscript certify that we have sufficiently participated in the work, including literature collection, interpretation, writing and revision of manuscript. Each author certifies that the work presented in the manuscript is not published or submitted in any other publication.

Conflicts of interest

The authors of this manuscript declare no conflicts of interest.

Appendix A. Supplementary data

Supplementary data to this article can be found online at https://doi.org/10.1016/j.bios.2019.111417.

References

Ahmad, R., Ahn, M.-S., Hahn, Y.-B., 2017a. J. Colloid Interface Sci. 498, 292–297.
Ahmad, R., Ahn, M.-S., Hahn, Y.-B., 2017b. Electrochem. Commun. 77, 107–111.
Ahmad, R., Tripathy, N., Jang, N.K., Khang, G., Hahn, Y.-B., 2015. Sens. Actuators, B 206, 146–151.
Alavi-Tabari, S.A.R., Khalilzadeh, M.A., Karimi-Maleh, H., 2018. J. Electroanal. Chem. 811, 84–88.
Ansari, A.A., Kaushik, A., Solanki, P.R., Malhotra, B.D., 2010. Bioelectrochemistry 77, 75–81.
Ansari, A.A., Singh, R., Sumana, G., Malhotra, B.D., 2009. Analyst 134, 997–1002.
Asikuzun, E., Ozturk, O., Arda, L., Terzioglu, C., 2018. J. Mol. Struct. 1165, 1–7.
Bajorowicz, B., Kobylański, M.P., Gołąbiewska, A., Nadolna, J., Zaleska-Medynska, A., Malankowska, A., 2018. Adv. Colloid Interface Sci. 256, 352–372.
Barrett, K.E., Boitano, S., Barman, S.M., Brooks, H.L., 2010. Ganong's Review of Medical Physiology. McGraw-Hill Companies, Inc.
Bukkitgar, S.D., Shetti, N.P., Kulkarni, R.M., Nandibewoor, S.T., 2015. RSC Adv. 5, 104891–104899.
Bukkitgar, S.D., Shetti, N.P., 2016. Mater. Sci. Eng. C 65, 262–268.
Bukkitgar, S.D., Shetti, N.P., 2017. Anal. Methods 9, 4387–4393.
Bukkitgar, S.D., Shetti, N.P., Kulkarni, R.M., 2018b. Sens. Actuators, B 255, 1462–1470.
Bukkitgar, S.D., Shetti, N.P., Kulkarni, R.M., Doddamani, M.R., 2016b. J. Electroanal. Chem. 762, 37–42.
Bukkitgar, S.D., Shetti, N.P., Kulkarni, R.M., Halbhavi, S.B., Wasim, M., Mylar, M., Durgi, P.S., Chirmure, S.S., 2016c. J. Electroanal. Chem. 778, 103–109.
Bukkitgar, S.D., Shetti, N.P., Kulkarni, R.M., Kulkarni, S.D., 2018. ECS J. Solid State Sci. Technol. 7, Q3215–Q3220.
Bukkitgar, S.D., Shetti, N.P., Kulkarni, R.M., Reddy, K.R., Shukla, S.S., Saji, V.S., Aminabhavi, T.M., 2019. J. Electrochem. Soc. 166, B3072–B3078.
Cha, X., Fan, Y., Chen, J., Wang, L., Xiang, Q., Duan, Z., Xu, J., 2018. Sens. Actuators, B 263, 436–444.
Cheraghi, S., Taher, M.A., Maleh, H.K., 2017. Appl. Surf. Sci. 420, 882–885.
Condello, M., Berardis, B.D., Ammendolia, M.G., Barone, F., Condello, G., Degan, P., Meschini, S., 2016. Toxicol in Vitro 35, 169–179.
Craddock, P.T., 2000. Years of Zinc and Brass, Rev ed. British Museum, London, pp. 27 1998.
Dai, Z., Shao, G., Hong, J., Bao, J., Shen, J., 2009. Biosens. Bioelectron. 24, 1286–1291.
Degen, A., Kosec, M., 2000. J. Eur. Ceram. Soc. 20, 667–673.
Devarushi, U.S., Shetti, N.P., Bukkitgar, S.D., Tuwar, S.M., 2018. Russ. J. Electrochem. 54, 760–768.
Dikovska, A.O., Pallotti, D., Lettieri, S., Atanasov, G.B., Avdeev, G.V., Maddalena, P., Amoruso, S., Nedyalkov, N.N., 2017. Appl. Surf. Sci. 423, 977–982.
Djurisic, A.B., Leung, Y.H., 2006. Small 2, 944–961.
Dong, S., Tong, M., Zhang, D., Huang, T., 2017. Sens. Actuators, B 251, 650–657.
Eadi, S.B., Duong, T.T., Kim, S., 2018. Superlattice. Microst. 120, 250–256.
Ebrahimi, M., Yousefzadeh, S., Samadi, M., Dong, C., Zhang, J., Moshfegh, A.Z., 2018. Appl. Surf. Sci. 435, 108–116.
Fan, D., Zhang, R., Zhu, Y., Peng, H., 2012. Physica B 407, 3510–3514.
Fan, L., Jiang, T., Xiao, T.T., Chen, J., Peng, L., Wang, X., Yan, D., Wu, W., 2018. J. Cryst. Growth 490, 6–10.
Farhat, O.F., Halim, M.M., Ahmed, N.M., Qaeed, M.A., 2016. Superlattice. Microst. 100, 1120–1127.
Fathil, M.F.M., Md Arshad, M.K., Ruslinda, A.R., Gopinath, S.C.B., Nuzaihan, M.N.,M., Adzhri, R., Hashim, U., Lam, H.Y., 2017. Sens. Actuators, B 242, 1142–1154.
Fei, J., Luo, D., Huang, J., Zhang, C., Duan, X., Zhang, L., 2018. Surf. Coating. Technol. 344, 433–440.
Fernandes, R.A., Sampaio, M.J., da Silva, E.S., Serp, P., Faria, J.L., Silva, C.G., 2019. Catal. Today 328, 286–292.
Fung, C.M., Lloyd, J.S., Samavat, S., Deganello, D., Teng, K.S., 2017. Sens. Actuators, B 247, 807–813.
Galdamez, A., Serrano, A., Santana, G., Arjona, N., Arriaga, L.G., Tapia Ramirez, J., Oza, G., Dutt, A., 2019. Mater. Lett. 235, 250–253.
Gao, X., Yue, H., Huanga, S., Lin, X., Gao, X.P.A., Wang, B., Yao, L., Wang, W., Guo, E., 2018. J. Electroanal. Chem. 808, 189–194.
Gasparotto, G., Costa, J.P.C., Costa, P.I., Zaghete, M.A., Mazon, T., 2017. Mater. Sci. Eng. C 76, 1240–1247.
Gong, B., Shi, T., Liao, G., Li, X., Huang, J., Zhou, T., Tang, Z., 2017. Appl. Surf. Sci. 406, 294–300.
Gu, B., Xu, C., Yang, C., Liu, S., Wang, M., 2011. Biosens. Bioelectron. 26, 2720–2723.
Haase, H., Ober-Blöbaum, J.L., Engelhardt, G., Hebel, S., Heit, A., Heine, H., Rink, L., 2008. J. Immunol. 181, 6491–6502.
Haque, E., Kim, J., Malgras, V., Reddy, K.R., Ward, A.C., You, J., Bando, Y., Hossain, S.A., Yamauchi, Y., 2018. Small Methods 1–14 1800050.
He, Y.B., Li, G.R., Wang, Z.L., Su, C.Y., Tong, Y.X., 2011. Energy Environ. Sci. 4, 1288–1292.
Hossein-Babaei, F., Akbari-Saatlu, M., 2017. Scripta Mater. 139, 77–82.
Hosseinzadeh, G., Maghari, A., Saboury, A.A., Moosavi-Movahedi, A.A., 2016. Int. J. Biol. Macromol. 86, 169–176.
Hu, Y.Y., Liu, Z., Nam, K.W., Borkiewicz, O.J., Cheng, J., Hua, X., Dunstan, M.T., Yu, X., Wiaderek, K.M., Du, L.S., Chapman, K.W., Chupas, P.J., Yang, X.Q., Grey, C.P., 2013. Nat. Mater. 12, 1130–1136.
Huang, J., Chen, F., Zhang, Q., Zhan, Y., Ma, D., Xu, K., Zhao, Y., 2015. ACS Appl. Mater. Interfaces 7, 5725–5735.
Iyer, M.A., Oza, G., Velumani, S., Maldonado, A., Romero, J., Mu˜noz, M.L., Sridharan, M., Asomoza, R., Yi, J., 2014. Sens. Actuators, B 202, 1338–1348.
Jali, M.H., Rahim, H.R.A., Johari, M.A., Thokchom, S., Harun, S.W., 2018. Sens. Actuators, A A. 277, 103–111.
Jang, E., Won, J., Kim, Y., Cheng, Z., Choy, J., 2010. J. Solid State Chem. 183, 1835–1840.
Ji, D., Fan, L., Li, L., Mao, N., Qin, X., Peng, S., Ramakrishna, S., 2018. Carbon 142, 379–387.
Jindal, K., Tomar, M., Gupta, V., 2017. Sens. Actuators, B 253, 566–575.
Jung, D.U.J., Ahmad, R., Hahn, Y.B., 2018. J. Colloid Interface Sci. 512, 21–28.
Karimi-Maleh, H., Tahernejad-Javazmi, F., Gupta, V.K., Malek, H.A., Asadi, H., 2014. J. Mol. Liq. 196, 258–263.
Kaur, M., Kailasaganapathi, S., Ramgir, N., Datta, N., Kumar, S., Debnath, A.K., Aswal, D.K., Gupta, S.K., 2017. Appl. Surf. Sci. 394, 258–266.
Ko, R.M., Lin, Y.R., Chen, C.Y., Tseng, P.F., Wang, S.J., 2018. Curr. Appl. Phys. 18, 1–11.
Kumar, P., Kumar, P., Deep, A., Bharadwaj, L.M., 2013. Appl. Nanosci. 3, 141–144.
Kumar, N.K.H., Devabrath, A.J., Manjunatha, S., Muralib, M., Amruthesh, K.N., Jagannath, S., 2019. Biocatal. Agric. Biotechnol. 18, 101024.
Lamson, T.L., Khan, S., Wang, Z., Zhang, Y., Yu, Y., Chen, Z., Xu, H., 2018. Optic Commun. 411, 53–58.
Li, J., Zhu, J.-J., 2013. Analyst 138, 2506.
Li, J., Zhang, W., Sun, J., 2016. Ceram. Int. 42, 9851–9857.
Li, K.H., Liu, X., Wang, Q., Zhao, S., Mi, Z., 2015. Nat. Nanotechnol. 10, 140–144.
Li, X., Xing, Y., Jiang, Y., Ding, Y., Li, W., 2009. Int. J. Food Sci. Technol. 44, 2161–2168.
Liu, A., Yin, K., Mi, L., Ma, M., Liu, Y., Li, Y., Wei, W., Zhang, Y., Liu, S., 2017. Anal. Chim. Acta 973, 82–90.
Liu, Y., Hu, W., Lu, Z., Li, C.M., 2014. ACS Appl. Mater. Interfaces 6, 7728–7734.
Lupan, O., Chow, L., Chai, G., 2009. Sens. Actuators, B 141, 511–517.
Medawar-Aguilar, V., Jofre, C.F., Fernández-Baldo, M.A., Alonso, A., Angel, S., Raba, J., Pereira, S.V., Messina, G.A., 2019. Anal. Biochem. 564–565, 116–122.
Meng, F., Zheng, H., Sun, Y., Li, M., Liu, J., 2017. Sensors 17, 1478–1491.
Migliorini, F.L., Sanfelice, R.C., Mercante, L.A., Andre, R.S., Mattoso, L.H.C., Correa, D.S., 2018. Appl. Surf. Sci. 443, 18–23.
Mishra, Y.K., Adelung, R., 2018. Mater. Today 21, 631–651.
Mohammed, A.M., Ibraheem, I.J., Obaid, A.S., Bououdina, M., 2017. Sens. Bio Sens. Res. 15, 46–52.
Mousavi, S.H., Haratizadeh, H., de Oliveira, P.W., 2012. Mater. Lett. 70, 86–88.
Moyo, M., Florence, L.R., Okonkwo, J.O., 2015. Sens. Actuators, B 209, 898–905.
Nandi, R., Major, S.S., 2017. Appl. Surf. Sci. 399, 305–312.
Nandi, S., Boruah, B.D., Misra, A., 2017. Sens. Actuators, A 267, 351–359.
Neveling, D.P., van den Heever, T.S., Perold, W.J., Dicks, L.M.T., 2014. Sens. Actuators, B 203, 102–110.

Ogata, K., Dobashi, H., Koike, K., Sasa, S., Inoue, M., Yano, M., 2010. Phys. E Low-dimens. Syst. Nanostruct. 42, 2880–2883.
Ouhenia-Ouadahi, K., Andrieux-Ledier, A., Richardit, J., Albouy, P.A., Beaunier, P., Sutter, P., Sutter, E., Courty, A., 2016. Chem. Mater. 28, 4380–4389.
Pahlavan, A., Gupta, V.K., Sanati, A.L., Karimi, F., Yoosefian, M., Ghadami, M., 2014. Electrochim. Acta 123, 456–462.
Park, Y., Yoo, R., Park, S., ryull, Lee, J.H., Jung, H., Lee, H.-S., Lee, W., 2019. Sens. Actuators, B 290, 258–266.
Patil, S.B., Naik, H.S.B., Nagaraju, G., Swamy, B.E.K., Reddy, K.R., 2018. Chem. Selct 3, 9025–9033.
Paul, K.B., Panigrahi, A.K., Singh, V., Singh, S.G., 2017. Analyst 142, 2128–2135.
Paul, K.B., Kumar, S., Tripathy, S., Vanjari, S.R.K., Singh, V., Singh, S.G., 2016. Biosens. Bioelectron. 80, 39–46.
Perrièrea, J., Jedrecya, N., Millon, E., Cachoncinlle, C., Talbi, A., Demange, V., Guilloux-Viry, M., Nisto, M., 2018. Thin Solid Films 652, 34–38.
Picciolini, S., Castagnetti, N., Vanna, R., Mehn, D., Bedoni, M., Gramatica, F., Villani, M., Calestani, D., Pavesi, M., Lazzarini, L., Zappettini, A., Morasso, C., 2015. RSC Adv. 5, 93644–93651.
Politi, J., Gioffrè, M., Rea, I., DeStefano, L., Rendina, I., 2015a. Proc. SPIE 9506, 1Z 1Z.
Politi, J., Rea, I., Dardanoa, P., De Stefano, L., Gioffrè, M., 2015b. Sens. Actuators, B 220, 705–711.
Preedia, B.E., Subastri, A., Suyavaran, A., Lokeshwara, R.P., Suresh, K.M., Jeevaratnam, K., Thirunavukkarasu, C., 2015. RSC Adv. 5, 62067–62077.
Preety, Hooda, V., 2018. Int. J. Biol. Macromol. 106, 1173–1183.
Qi, J., Chang, J., Han, X., Zhong, R., Jiang, M., Chen, Z., Liu, B., 2018. Mater. Chem. Phys. 211, 168–171.
Qu, X., Yang, R., Tong, F., Zhao, Y., Wang, M., 2018. Powder Technol. 330, 259–265.
Qu, X., Lu, S., Wang, J., Li, Z., Xue, H., 2012. Mater. Sci. Semicond. Process. 15, 244–250.
Rahmanian, R., Mozaffari, S.A., Amoli, H.S., Abedi, M., 2018. Sens. Actuators, B 256, 760–774.
Reddy, K.R., Jeong, H.M., Lee, Y., Raghu, A.V., 2010. J. Polym. Sci., Part A: Polym. Chem. 48, 1477–1484.
Reddy, K.R., Sin, B.Y., Noh, J., Lee, Y., 2009a. Synth. Met. 159, 1934–1939.
Reddy, K.R., Sin, B.Y., Park, W., Ryu, K.S., Chung, H., Lee, Y., 2009b. Synth. Met. 159, 595–603.
Rodrigues, A., Carmo, M.do, Alves, M., Morais, J., 2018. Mater. Des. 142, 240–246.
Sahdev, P., Podaralla, S., Kaushik, R.S., Perumal, O., 2013. J. Biomed. Nanotechnol. 9, 132–141.
Sankapal, B.R., Gajare, H.B., Karade, S.S., Salunkhe, R.R., Dubal, D.P., 2016. Electrochim. Acta 192, 377–384.
Sarkar, D., Liu, W., Xie, X., Anselmo, A.C., Mitragotri, S., Banerjee, K., 2014. ACS Nano 8, 3992–4003.
Satish, T., Balakrishnan, K., Gullapalli, H., Nagarajaiah, S., Vajtai, R., Ajayan, P.M., 2017. Struct. Monit. Maint. 4, 107–113.
Selvarajan, S., Suganthi, A., Rajarajan, M., 2018. J. Phys. Chem. Solids 121, 350–359.
Shetti, N.P., Nayak, D.S., Kuchinad, G.T., Naik, R.R., 2018. Electrochim. Acta 269, 204–211.
Shetti, N.P., Nayak, D.S., Malode, S.J., Kakarla, R.R., Shukla, S.S., Aminabhavi, T.M., 2019a. Anal. Chim. Acta 1051, 58–72.
Shetti, N.P., Nayak, D.S., Malode, S.J., Kakarla, R.R., Shukla, S.S., Aminabhavi, T.M., 2019b. Colloids Surf., B 177, 407–415.
Shetti, N.P., Bukkitgar, D.B., Reddy, K.R., Reddy, V.C., Aminabhavi, T.M., 2019c. Colloids Surf., B 178, 385–394.
Shrestha, B.K., Shrestha, S., Tiwari, A.P., Kim, J.-I., Ko, S.W., Kim, H.-J., Park, C.H., Kim, C.S., 2017. Mater. Des. 133, 69–81.
Shukla, S., Sharma, N.K., Sajal, V., 2015. Sens. Actuators, B 206, 463–470.
Singhal, C., Pundir, C.S., Narang, J., 2017. Biosens. Bioelectron. 97, 75–82.
Sombrio, G., Rivaldo-Gómez, C.M., Pomar, C.A.D., Souza, J.A., 2017. Superlattice. Microst. 112, 180–185.
Son, D.Y., Im, J.H., Kim, H.S., Park, N.G., 2014. J. Phys. Chem. C 118, 16567–16573.
Song, L., Yue, H., Li, H., Liu, L., Li, Y., Du, L., Duan, H., Klyui, N.I., 2018. Chem. Phys. Lett. 699, 1–7.
Sun, X., Li, Q., Jiang, J., Mao, Y., 2014. Nanoscale 6, 8769–8780.
Tak, M., Gupta, V., Tomar, M., 2014. Biosens. Bioelectron. 59, 200–207.
Tak, M., Gupta, V., Tomar, M., 2017. J. Electroanal. Chem. 792, 8–14.
Tan, S.L.J., Webster, R.D., 2012. J. Am. Chem. Soc. 134, 5954–5964.
Tariq, M., Kasi, J.K., Samiullah, Kasi, A.K., 2018. Int. J. Chem. Mater. Eng. 12, 571–574.
Tereshchenko, A., Fedorenko, V., Smyntyna, V., Konup, I., Konup, A., Eriksson, M., Yakimova, R., Ramanavicius, A., Balme, S., Bechelany, M., 2017. Biosens. Bioelectron. 92, 763–769.
Thongsuksai, W., Panomsuwan, G., Rodchanarowa, A., 2018. Mater. Lett. 224, 50–53.
Urgessa, Z.N., Botha, J.R., Djiokap, S.R.T., Coleman, C., Bhattacharyya, S., 2018. Phys. B (Amsterdam, Neth.) 535, 79–83.
Urgessa, Z.N., Oluwafemi, O.S., Olivier, E.J., Neethling, J.H., Botha, J.R., 2013. J. Alloy. Comp. 580, 120–124.
Wang, H., Lee, H.W., Deng, Y., Lu, Z., Hsu, P.C., Liu, Y., Lin, D., Cui, Y., 2015a. Nat. Commun. 6, 7261–7268.
Wang, M., Xu, J., Sun, T., Tang, Y., Jiang, G., Shi, Y., 2018. Mater. Lett. 219, 236–239.
Wang, X., Sun, F., Duan, Y., Yin, Z., Luo, W., Huang, Y., Chen, J., 2015b. J. Mater. Chem. C. 3, 11397–11405.
Wang, X., Yu, H., Lu, D., Zhang, J., Deng, W., 2014. Sens. Actuators, B 195, 630–634.
Wang, Y., Deng, H., Huangfu, C., Lu, Z., Wang, X., Zeng, X., He, H., Rao, H., 2015c. Surf. Interface Anal. 47, 245–252.
Wu, J.Y., Hsu, K.-Y., 2015. J. Mol. Struct. 1099, 142–148.
Wu, Z.W., Tyan, S.L., Lee, C.R., Mo, T.S., 2017. Thin Solid Films 621, 102–107.
Xie, T., Song, S., Schwenke, K., Singh, M., Gonzalez, L.E., Gado, E.D., Hahm, J.I., 2015. Langmuir 31, 10493–10499.
Xu, J., Bertke, M., Gad, A., Yu, F., Hamdana, G., Bakin, A., Peiner, E., 2017. Eurosensor Proc. 4, 290.
Yildirim, O.A., Liu, Y., Petford-Long, A.K., 2015. J. Cryst. Growth 430, 34–40.
Yin, B., Qiu, Y., Zhang, H., Lei, J., Chang, Y., Ji, J., Luo, Y., Zhao, Y., Hu, L., 2015. RSC Adv. 5, 11469–11474.
Zhang, Q., Bai, W., 2011. Vacuum 86, 398–402.
Zhang, X., Dong, Z., Liu, S., Shi, Y., Dong, Y., Feng, W., 2017. Sens. Actuators, B 243, 1224–1230.
Zhang, X., Li, W., Zhou, Y., Chai, Y., Yuan, R., 2019. Biosens. Bioelectron. 135 8-3.
Zhou, C., Xu, L., Song, J., Xing, R., Xu, S., Liu, D., Song, H., 2014. Sci. Rep. 4, 7382–7390.
Zong, X., Zhu, R., 2018. Sens. Actuators, B 255, 2448–2453.